Blocking tumor-educated MSC paracrine activity halts osteosarcoma progression

S. Rubina Baglio[1]*, Tonny Lagerweij[2], Maria Pérez Lanzón[1], Xuan Dung Ho[3,4], Nicolas Léveillé[5], Sonia A. Melo[6], Anne-Marie Cleton-Jansen[7], Ekaterina S. Jordanova[8], Laura Roncuzzi[9], Michelina Greco[9], Monique A. J. van Eijndhoven[1], Giulia Grisendi[10], Massimo Dominici[10], Roberta Bonafede[1], Sinead M. Lougheed[11], Tanja D. de Gruijl[11], Nicoletta Zini[12,13], Silvia Cervo[14,15], Agostino Steffan[14,15], Vincenzo Canzonieri[14,16], Aare Martson[17], Katre Maasalu[17], Sulev Köks[3,18], Tom Wurdinger[2], Nicola Baldini[9,19]*, D. Michiel Pegtel[1]*.

[1] Department of Pathology, Cancer Center Amsterdam, VU University medical center, Amsterdam, The Netherlands.

[2] Department of Neurosurgery, Cancer Center Amsterdam, VU University medical center, Amsterdam, The Netherlands.

[3] Department of Pathophysiology, University of Tartu, Tartu, Estonia.

[4] Department of Oncology, Hue College of Medicine and Pharmacy, Hue University, Hue, Vietnam.

[5] Laboratory for Experimental Oncology and Radiobiology, Center for Experimental Molecular Medicine (CEMM), Academic Medical Center (AMC), Amsterdam, The Netherlands.

[6] Instituto de Investigação e Inovação em Saúde, Universidade do Porto, Portugal (i3S), Porto, Portugal; Institute of Pathology and Molecular Immunology of the University of Porto (IPATIMUP), Porto, Portugal; Department of Pathology, Faculty of Medicine of Porto University, Porto, Portugal.

[7] Department of Pathology, Leiden University Medical Center, Leiden, The Netherlands.

[8] Department of Obstetrics and Gynecology, Center for Gynaecological Oncology Amsterdam, VU University Medical Center, Amsterdam, The Netherlands.

[9] Orthopaedic Pathophysiology and Regenerative Medicine Unit, Istituto Ortopedico Rizzoli, Bologna, Italy.

[10] Division of Oncology, Department of Medical and Surgical Sciences for Children & Adults, University-Hospital of Modena and Reggio Emilia, Modena, Italy.

[11] Department of Medical oncology, Cancer Center Amsterdam, VU University medical center, Amsterdam, The Netherlands.

[12] CNR - National Research Council of Italy, Institute of Molecular Genetics, Bologna, Italy.

[13] Laboratory of Musculoskeletal Cell Biology, Rizzoli Orthopaedic Institute, Bologna, Italy.

[14] CRO-Biobank, CRO Aviano National Cancer Institute, Aviano, Italy.

[15] Clinical Cancer Pathology, CRO Aviano National Cancer Institute, Aviano, Italy.

[16] Pathology Unit, CRO Aviano National Cancer Institute, Aviano, Italy.

[17] Department of Traumatology and Orthopedics, University of Tartu, Tartu, Estonia.

[18] Department of Reproductive Biology, Estonian University of Life Sciences, Tartu, Estonia.

[19] Department of Biomedical and Neuromotor Sciences, University of Bologna, Bologna, Italy.

*To whom correspondence should be addressed: Serena Rubina Baglio, VU University medical center, de Boelelaan 1117, 1081HV Amsterdam (The Netherlands). Tel. +31 (0)20 4444052. Email: s.baglio@vumc.nl; Nicola Baldini, Istituto Ortopedico Rizzoli, via di Barbiano, 1/10, 40136 Bologna (Italy). Tel. +39 051 6366748.

Email: nicola.baldini@ior.it; D. Michiel Pegtel, VU University medical center, de Boelelaan 1117, 1081HV Amsterdam (The Netherlands). Tel. +31 (0)20 4444052. Email: d.pegtel@vumc.nl.

The authors have declared that no conflict of interest exists.

Abstract

PURPOSE: Human osteosarcoma is a genetically heterogeneous bone malignancy with poor prognosis despite the employment of aggressive chemotherapy regimens. Because druggable driver mutations have not been established, dissecting the interactions between osteosarcoma cells and supporting stroma may provide insights into novel therapeutic targets.

EXPERIMENTAL DESIGN: By using a bioluminescent orthotopic xenograft mouse model of osteosarcoma we evaluated the effect of tumor extracellular vesicle (EV)-educated mesenchymal stem cells (TEMSCs) on osteosarcoma progression. Characterization and functional studies were designed to assess the mechanisms underlying MSC education. Independent series of tissue specimens were analyzed to corroborate the preclinical findings, and the composition of patient serum EVs was analyzed after isolation with size-exclusion chromatography.

RESULTS: We show that EVs secreted by highly malignant osteosarcoma cells selectively incorporate a membrane-associated form of TGFB, which induces pro-inflammatory IL-6 production by MSCs. TEMSCs promote tumor growth, accompanied with intratumor STAT3 activation and lung metastasis formation, which was not observed with control MSCs. Importantly, intravenous administration of the anti-IL-6 receptor antibody tocilizumab abrogated the tumor-promoting effects of TEMSCs. RNA-seq analysis of human osteosarcoma tissues revealed a distinct TGFB-induced pro-metastatic gene signature. Tissue microarray immunostaining indicated active STAT3 signaling in human osteosarcoma, consistent with the observations in TEMSC-treated mice. Finally, we isolated pure populations of EVs from serum and demonstrated that circulating levels of EV-associated TGFB are increased in osteosarcoma patients.

CONCLUSION: Collectively, our findings suggest that TEMSCs promote osteosarcoma progression and provide the basis for testing IL-6 and TGFB blocking agents as new therapeutic strategies for osteosarcoma patients.

Statement of translational relevance

Osteosarcoma is a highly aggressive bone tumor of childhood and adolescence for which alternative therapeutic options are urgently needed. We demonstrate that osteosarcoma cells release TGFβ-rich extracellular vesicles (EVs) inducing a pro-metastatic phenotype characterized by high IL-6 production in mesenchymal stem cells (MSCs). Administration of the IL-6R antibody tocilizumab prevents lung metastasis formation induced by the tumor-educated MSCs in an orthotopic xenograft model of osteosarcoma. We found evidence of active TGFβ and stroma-dependent IL-6 signaling in osteosarcoma patients, who in addition display high circulating levels of EV-associated TGFβ compared to control individuals. Our study provides a rationale for the use of IL-6R antibodies, possibly in combination with TGFβ blocking agents, as a new therapeutic strategy to stop osteosarcoma progression.

Running title

Osteosarcoma EVs trigger pro-metastatic IL-6 production by MSCs

Introduction

Osteosarcoma is a very aggressive bone tumor, which mainly affects children and adolescents. Lung metastases are present in approximately 20% of osteosarcoma patients at diagnosis and represent the main cause of death. However, undetectable micrometastases seem to be present in at least 80% of patients at initial diagnosis, and they are mostly resistant to the aggressive chemotherapy regimen used for osteosarcoma (1). As a consequence, the 5-year survival rate in the presence of metastatic disease does not exceed 20% (2). The rarity and heterogeneity of osteosarcoma, together with the chaotic genomic rearrangements and exceptionally frequent chromotripsis (3), are major obstacles in the search for molecular therapeutic targets. Indeed, no improvements in osteosarcoma survival have been achieved in the last 30 years (2). Recent studies pointed to a defining role for the local and systemic environment in osteosarcoma initiation and progression (4,5). Osteosarcoma develops during the adolescent growth spurt at sites of rapid bone growth, and preferentially affects male individuals that are taller for their age (6,7). Intercepting the environmental factors sustaining osteosarcoma may halt or even reverse malignant progression thereby providing novel therapeutic options.

The tumor microenvironment takes part in virtually every aspect of cancer development and progression (8). Mesenchymal stem cells (MSCs) are established contributors to malignant dissemination in multiple cancer types including breast cancer, brain tumors, colon cancer and osteosarcoma (9–12). MSCs are adult stem cells that home to sites of inflammation, where in response to environmental cues they can differentiate into cancer-supporting cells. Cancer-associated MSCs provide essential factors for malignant progression (13). MSC-derived CCL5 promotes metastasis formation in breast and prostate cancer (9,14), interleukin-6 (IL-6) released by MSCs supports tumor growth and angiogenesis in colorectal cancer (15), and MSC-derived stromal derived growth factor-1 (SDF-1) favors epithelial-mesenchymal transition (EMT) and metastasis in prostate cancer (16). However, how tumor cells influence MSC behavior to favor metastatic progression is not understood.

Tumor cells are prolific producers of extracellular vesicles (EVs), including a significant proportion of vesicles of endosomal origin called exosomes (17). Exosomes are 40–100 nm vesicles carrying a bioactive cargo of the cell of origin, including proteins, lipids and regulatory RNAs (18). In addition, tumor cells shed membrane vesicles from their surface that are difficult to distinguish from exosomes based on protein content (19). Therefore we will refer to the heterogeneous population of vesicles released by cancer cells using the term EVs. Once released, EVs can be taken up by surrounding cells or carried to distant sites via the blood or lymph circulation and influence target cell behavior (18,20,21). Cancer EVs can transport functional RNAs that promote angiogenesis (22), oncoproteins involved in pre-metastatic niche formation (20), and heat-shock proteins that can suppress anti-tumor immune responses (23). Circulating tumor EVs can be detected in cancer patients and have remarkable diagnostic and prognostic potential (24) and may predict response to treatment (25).

We provide evidence that osteosarcoma-produced EVs trigger a pro-metastatic inflammatory loop by altering the physiology of MSCs. We reveal that EVs from metastatic osteosarcoma cells carry a membrane-associated form of TGFβ that educates human MSCs to produce IL-6 in vitro. When injected in a pre-clinical mouse model, “tumor-educated” MSCs (TEMSCs) promote osteosarcoma growth and lung metastasis formation. Importantly, co-administration of a therapeutic IL-6 receptor (IL-6R) antibody abolishes the cancer-promoting effects of TEMSCs. Our study reveals IL-6 and TGFβ as rational targets for therapeutic intervention in osteosarcoma patients.

Methods

Clinical specimens

Tissue microarrays from paraffin embedded tumor tissue were previously constructed (26). All specimens were handled according to the ethical guidelines described in Code for Proper Secondary Use of Human Tissue in The Netherlands of the Dutch Federation of Medical Scientific Societies. Immunohistochemistry was performed as described previously (27). The Phospho-STAT3(Tyr705)(D3A7) antibody (Cell Signaling Technology) was used at a 1:400 dilution. Lung carcinoma tissue was used as a positive control for titration. Cores from 103 tumor tissues were scored by staining intensity and percentage of positive cells (average scores from 3 cores/tumor were calculated), and the percentage of pSTAT3 positive tumors was calculated (cut-off value: 5% positive cells/tumor tissue). The analysis was performed by two operators independently.

OS tissues for RNA-seq analysis were collected from eighteen patients in Vietnam who had histologically confirmed osteosarcoma and were allocated for surgery. Tumor and normal bone samples were collected from the removed bone immediately after the operation. Samples were stored at -80°C until RNA extraction. Protocols were approved from the ethics committee on biomedical research of the Hue University hospital. All the participants or representative of patients signed the informed consent.

Serum samples used in this study were prepared and stored by CRO-Biobank (CRO National Cancer Institute, Aviano, Italy). The CRO-Biobank project has been approved by the CRO Institutional Ethics Committee and all participants provided written informed consent. Briefly, blood samples were collected in Serum Z tubes (Monovette®, Sarstedt), placed on ice and centrifuged at 2608 g for 10 minutes at room temperature. Aliquots of serum were then stored at -80°C.

All clinical samples used in this study were used in compliance with the Declaration of Helsinki.

Cell culture

Human adipose tissue samples were obtained from the department of Plastic Surgery of the Tergooi Hospital (Hilversum, the Netherlands) after institutional Ethical committee approval and written informed consent. MSCs were isolated as previously described (28). GFP-positive adipose-derived MSCs were obtained from the Department of Medical and Surgical Sciences for Children and Adults (University of Modena and Reggio Emilia, Italy) (29). MSCs were expanded in alpha-MEM (Lonza), supplemented with 5% platelet Lysate and 10 U/ml heparin (Leo Pharma). MG63, HOS and 143B osteosarcoma cells were cultured in IMDM supplemented with 10% FBS. Primary human fibroblasts were a kind gift of JM Middeldorp (VUmc, Amsterdam) and were cultured in DMEM 10% FBS. Primary osteosarcoma cells were kindly provided by VW van Beusechem (VUmc, Amsterdam) and cultured in EMEM 10% FBS. All media were supplemented with 100 U/ml penicillin and 100 µg/ml streptomycin (Gibco).

The endolysosomal compartment of osteosarcoma cell lines was characterized by confocal laser scanning microscopy and transmission electron microscopy (TEM) as previously described (28).

For cell cycle analysis MSCs were exposed to osteosarcoma or control EVs for 48 hours (two EV treatments) and incubated overnight with nocodazole (250 ng/ml) to arrest them in G2/M. The following day cells were collected, washed and resuspended in PBS containing 0.6% NP-40, 50 mg/ml RNaseA and 50 mg/ml propidium iodide for 10 min, and analyzed using a FACS Calibur flow cytometer (BD Biosciences). For the osteogenic differentiation assay MSCs were cultured in the presence of 0.1 M ascorbic acid and 10^{-8}M dexamethasone. At

cell confluence 10mM β-glycerophosphate was added to the cultures, and after one week mineral deposition was assessed by Alizarin red staining.
To evaluate whether IL-6 induction in MSCs was dependent on the EV RNA, MSCs were seeded in 12-well plates at a density of 70.000 cells/well. The day after cells were transfected with EV-RNA or 20ng Poly I:C (Sigma-Aldrich) (positive control) using lipofectamine 2000 (Life Technologies), or treated with matching amounts of osteosarcoma EVs. 48 hours after transfection, MSCs were lysed in TRIzol (Life Technologies) for IL-6 expression analysis.
To assess whether IL-6 induction was dependent on TGFβ signaling, MSCs were pre-incubated for 30 minutes with the activin receptor-like kinase (ALK) receptor inhibitor SB-431542 (Sigma-Aldrich) at a concentration of 10 µM and then exposed to osteosarcoma EVs or 5ng/ml soluble human TGF-β (ProSpec). A second EV/TGF-β treatment was performed after 24h. At 24h and 48h cells were lysed in TRIzol for mRNA expression analysis. The MSC conditioned medium was harvested to perform IL-6 ELISA.

Exosome isolation and characterization

EVs were isolated from the culture supernatant using differential centrifugation (28). EVs preparations and corresponding cells of origin were characterized by western blot for enriched EV proteins as CD63 and CD81 and by TEM, and the EV RNA profile was analyzed using the Bioanalyzer (Agilent) as previously described (28).
Vesicle internalization after staining with PKH67 (Sigma-Aldrich) was assessed by fluorescence microscopy and FACS analysis. To inhibit EV internalization cells were were pre-incubated for 30 minutes with 50µM dynasore (Sigma-Aldrich).
EVs from serum were purified by size-exclusion chromatography (SEC) as previously described (30). Fractions 9 and 10 were considered as as EV-enriched fractions, and subjected to TGFβ protein quantification by ELISA.

Cytometric bead array and ELISA

Quantification of a panel of inflammatory cytokines was performed using the BD™ Cytometric Bead Array (CBA) Human Inflammatory Cytokines Kit (BD Biosciences) following the manufacturer's instructions.
IL-6 and TGFβ protein concentration were assessed using the Human IL-6 and Human TGF-beta 1 DuoSet ELISA (R&D systems) respectively. Quantification of soluble IL-6R was carried out using the Human IL-6 R alpha Quantikine ELISA Kit (R&D systems), according to the manufacturer´s instructions.

RNA isolation and qPCR

Total RNA was isolated using Trizol Reagent (Life Technologies). Exosome preparations were pre-treated with RNase A (Sigma-Aldrich) at a final concentration of 400 ng/µl at 37°C for 1 hour to degrade unprotected RNAs. IL-6 mRNA expression was analyzed using SYBR Green PCR master mix in a LightCycler 480 Real-time PCR System (Roche) with the following primer sets:
IL-6-F: 5'-AGTGAGGAACAAGCCAGAGC-3'; IL-6-R: 5'-CATTTGTGGTTGGGTCAGG-3'.
The mRNA expression of TLR3, TLR7, TLR8 and TLR9 was analyzed using the Universal ProbeLibrary system (Roche Applied Science). Probes and primers were selected using the web-based ProbeFinder software. Results were normalized to GAPDH.

Animal experiments

Animal experiments were performed in accordance with the Dutch law on animal experimentation with the approval of the Committee on animal experimentation of the VU University medical center (Amsterdam, The Netherlands).

For orthotopic tumor xenografting, a single cell suspension of exponentially growing luciferase-positive 143B cells was injected into the tibia of nude mice. Briefly, six-weeks old Athymic Nude-Foxn1^{nu} mice (Harlan) (n=6 per treatment arm) received buprenofine s.c. (0.05 mg/kg) and were anesthetized with isoflurane (2-3% in oxygen). After anesthesia the knee was flexed beyond 90°, a skin incision was made to expose the tibia and a pinhole was made using a 0.8 mm drill. A volume of 1 µl cell suspension (approximately 2 x 10^5 cells), was injected into the hole using a 25 gauge needle. The hole was closed with tissue glue to prevent backflow, and the skin was closed with sutures. The anti-IL-6R antibody tocilizumab (100 µg/mouse, i.p.) was administered at day 1 and every other day until the experimental endpoint. Control animals were treated with PBS. One million GFP-positive MSCs educated or not educated with osteosarcoma EVs were injected i.v. (100 µl) at day 2. Tumor growth was monitored by BLI. Briefly, 150 µl D-luciferin (0.03 g/L, Gold Biotechnoloby) was injected intraperitoneally, and 10 minutes after administration mice were anesthetized with isoflurane and positioned in the IVIS camera. The bioluminescence signal was determined with the IVIS Lumina CCD camera. Mice were monitored daily for discomfort and weight loss. When the first animal presented moderate to severe symptoms of discomfort (weight loss of >15% or tumor diameter >15 mm), all animals were sacrificed. The duration of the experiments was approximately 3 weeks. BLI of the ex vivo tissues was measured with the IVIS, and tissues were formalin-fixed or cryopreserved for histological analysis. Two animal experiments with 6 mice/experimental group were performed. In figure 2 results from both experiments were pooled. Figure 5 shows the results of the second experiment only.

Immunohistochemical and immunofluorescent analysis

Immunohistochemical analysis of FFPE mouse tissue (lung) slides was performed according to standard protocols. Briefly, heat-mediated antigen retrieval was performed using citrate buffer. Slides were incubated with the Vimentin antibody (V9) (Santa Cruz) diluted 1:150, and counterstained with hematoxylin.

To assess the presence of GFP-positive MSCs in tumor and bone marrow tissues, mouse tibias were decalcified in EDTA pH 7.2-7.4. Antigen retrieval was performed using citrate buffer. Tissue slides were stained with a rabbit polyclonal anti-GFP antibody (Abcam, ab290) in a 1:900 dilution, and counterstained with DAPI.

For the pSTAT3 staining of FFPE osteosarcoma xenograft slides, antigen retrieval was performed with a TRIS-EDTA buffer pH 9, and slides were incubated with the Phospho-STAT3(Tyr705)(D3A7) (1:100) and with the goat-anti-rabbit-Alexa 546 (Life Technologies) (1:200) antibodies and counterstained with DAPI. Images were acquired with an LSM700 confocal laser scanning microscope equipped with an LCI Plan-Neofluar 25x/0.8 Imm Korr DIC M27 objective (Zeiss). Positivity was determined using the LSM Image Browser (version 4.2.0.121, Zeiss).

RNA sequencing

Bone samples (40-50 mg) were grinded into powder with nitrogen in a mortar and lysed using TRIzol. Total RNA was extracted with RNeasy Fibrous Tissue Mini Kit (Qiagen) according to the manufacturer's protocol. The quality of total RNA was assessed with Agilent 2100 Bioanalyzer using the RNA 6000 Nano Kit (Agilent Technologies). 50 ng of total RNA was amplified by applying Ovation RNA-Seq System V2 (NuGen). The

resulting cDNAs were pooled in equal amounts and the DNA fragment library was prepared with SOLiD System chemistry (Life Technologies). Sequencing was performed using SOLiD 5500W platform and DNA sequencing chemistry (Life Technologies). Raw reads (75 bp) were color-space mapped to the human genome hg19 reference using Maxmapper algorithm implemented in the Lifescope software (Life Technologies). Mapping to multiple locations was permitted. The quality threshold was set to 10, giving the mapping confidence was more than 90. Reads with score less than 10 were filtered out. Average mapping quality was 30. Analysis of the RNA content and gene-based annotation was done within whole transcriptome workflow. For statistical analysis DeSeq2 package for R was used (31).

Statistics

Statistical analysis was performed using the IBM SPSS statistics software. Data were expressed as means ± standard deviation or standard error of the mean (SEM). Two-tailed t test and one-way ANOVA were applied to assess the effects of independent variables on quantitative results. The post-hoc Fisher's Least Significant Difference (LSD) test was applied to highlight the differences between individual groups. P values ≤ 0.05 were considered statistically significant.

Results

Osteosarcoma cells release exosome-like EVs that are efficiently internalized by MSCs

To study the EV population released by osteosarcoma cells we used two non-metastatic (MG-63 and HOS) and one metastatic (143B) osteosarcoma cell lines. We first analyzed the cellular endosomal compartment by immunofluorescent staining for CD63. We found high punctate expression of CD63, localized both in acidic and non-acidic vesicles throughout the cell body as determined by lysotracker co-staining (Figure 1a, top). By transmission electron microscopy (TEM) we revealed the presence of multiple 500nm late endosomes with internal vesicular structures of 40-100nm (Figure 1a, bottom), resembling multivesicular bodies (MVB).

We then isolated osteosarcoma EVs using differential centrifugation. The purity of the preparations was confirmed by TEM (Figure 1b) and western blot for the exosomal proteins CD63 and CD81 (Figure 1c). TEM analysis of cell compartments and purified vesicles suggests that osteosarcoma cells release greater amount of EVs compared to their normal counterparts (bone marrow-MSCs) we previously analyzed (28).

To investigate whether osteosarcoma EVs can interact with MSCs, we labeled purified vesicle preparations with a fluorescent lipid dye (PKH67) prior to incubation with MSCs. After 24 hours we observed EV internalization by fluorescence microscopy and FACS analysis (Figure 1d and Supplementary figure 1). To identify non-malignant vesicles that could be used as controls for following assays we evaluated the ability of MSCs to internalize human fibroblast (hF) and MSC EVs. We found that the uptake efficiencies of osteosarcoma EVs (96.9-99.2% positive cells) and control EVs (93.3-99.2% positive cells) were highly similar (Supplementary figure 1). These observations suggest that besides phagocytic cells, as dendritic cells and macrophages (32,33), human primary MSCs efficiently capture and internalize EVs from various cell types including tumor (OS) cells.

Tumor-educated MSCs promote osteosarcoma growth and lung metastasis formation

To investigate whether osteosarcoma EVs alter the physiology of MSCs such that they promote tumor progression, we developed a bioluminescent orthotopic xenograft mouse model of osteosarcoma. Human primary GFP-positive MSCs were expanded and exposed for 48 hours to EVs purified from metastatic 143B cells. Metastatic luciferase-positive 143B cells were inoculated in the tibia of nude mice, and after 2 days the osteosarcoma-bearing mice were subjected to a single systemic administration of “tumor-educated” MSCs (TEMSCs) (Figure 2a). Mice receiving non-educated MSCs or no MSCs were used as control groups. Tumor growth was monitored by bioluminescence imaging (BLI). As early as day 10 after inoculation we observed increased tumor growth in mice that received TEMSCs compared to the control groups. The difference in tumor volume became increasingly prominent at the following time-points (Figure 2b,c).

The dynamics of the tumor microenvironment seem to have features of a wound healing process (34), including the recruitment of MSCs (35). We searched for the presence of GFP-positive MSCs in decalcified mouse tibias four days after systemic injection, and found GFP-positive cells within the tumor mass and in the adjacent bone-marrow tissue of mice receiving TEMSCs and control MSCs (Figure 2d).

Next we investigated whether TEMSCs promote osteosarcoma metastatic progression. Ex vivo BLI of lungs, liver and spleen (Figure 2e) revealed that metastatic dissemination exclusively occurred in the lungs, the most common metastatic sites in osteosarcoma patients. The number of lung metastases across the experimental groups was determined by BLI and naked eye evaluation. Strikingly, administration of TEMSCs significantly increased the number of metastases compared to the control groups (Figure 2f). The presence of metastases in

the lungs was confirmed by human vimentin staining (Figure 2g). No GFP-positive MSCs were detected in the lung tissue at the experimental endpoint.
Collectively these observations demonstrate that osteosarcoma EVs prompt MSCs to acquire a pro-tumorigenic and pro-metastatic phenotype in vivo.

OS EVs induce IL-6 production and stimulate cell cycle progression in human primary MSCs

Because MSCs have specialized immuno-modulatory functions (36), we wondered whether osteosarcoma EVs affect cytokine production by MSCs. We used a multiplexed bead-based assay to profile the cytokine production of MSCs upon treatment with EVs. Interestingly, we observed that education of human primary MSCs with EVs from the metastatic 143B cells increased the production of IL-6 and IL-8 when compared to control EVs (Figure 3a and Supplementary Figure 2a). We noticed that osteosarcoma cell lines and primary osteosarcoma cells release IL-8, but do not produce detectable levels of IL-6 (Figure 3b and Supplementary figure 2b,c). Therefore we postulated that MSCs may act as tumor-supporting stroma cells by supplying exogenous IL-6 in vivo. We confirmed that 143B EVs educate MSCs to produce IL-6 both at the mRNA (Supplementary Figure 2d) and protein level (Figure 3c). The responsiveness of target cells to IL-6 depends either on the expression of the surface IL-6 receptor (IL-6R) or on the availability of a soluble form of the IL-6R (sIL-6R). While the expression of the surface IL-6R is limited to few cell types in vivo, we found that both osteosarcoma cells and MSCs produce sIL-6R (Figure 3d). The production of sIL-6R by MSCs was however not influenced by treatment with osteosarcoma EVs (Supplementary figure 2e). Taken together these findings demonstrate that osteosarcoma cells release EVs inducing IL-6 production in MSCs, and can respond to MSC-derived IL-6 in a cell-autonomous fashion.

Because IL-6 is implicated in proliferation and stemness maintenance of MSCs (37), we investigated the effects of osteosarcoma EVs on cell cycle progression and osteogenic differentiation of these cells. We cultured MSCs in the presence of osteosarcoma EVs for 48h and then treated cells with nocodazole overnight to prevent mitosis. FACS analysis showed that 143B EVs determined greater accumulation of cells in the G2/M phase compared to control EVs or untreated condition (set at 0) (Figure 3e,f), suggesting that osteosarcoma EVs accelerate the transition from G1 to G2/M. To study whether EVs affect the differentiation of MSCs we cultured early passage MSCs in osteogenic conditions and evaluated the formation of mineral nodules with Alizarin red staining (Supplementary figure 2f). No differences were observed in response to osteosarcoma EV treatment, suggesting that osteosarcoma EVs promote cell cycle progression, but do not affect the osteogenic differentiation ability of MSCs.

OS EV-associated TGFβ induces IL-6 expression in MSCs

OS EVs induce IL-6 release and cell-cycle progression in MSCs, but the mechanism underlying these effects is unclear. One possibility is that osteosarcoma EVs transfer inflammatory small RNAs that are recognized by intracellular sensors within the endosomal compartments of the MSCs (32,38,39). We extracted RNA from osteosarcoma EVs and analyzed their small RNA profile using the Bioanalyzer. The small RNA profile showed characteristic exosomal RNA peaks between 20 and 70 nt (Figure 4a). RNA-seq analysis revealed high abundance of polymerase III transcripts (data not shown), which can induce inflammatory responses in recipient cells (32,39). We then determined the expression of endosomal Toll-like receptors (TLRs) in MSCs (Figure 4b), and transfected cells with the RNA isolated from osteosarcoma EVs (EV-RNA). While MSCs strongly

responded to the TLR3 agonist poly(I:C), no effect on IL-6 expression was observed in response to isolated EV-RNA (Figure 4c, left). However, a single treatment with matching amounts of intact tumor EVs prompted a 2-fold increase in IL-6 mRNA expression (Figure 4c, right). These observations suggest that EV components other than RNAs induce IL-6 production in recipient MSCs.
One emerging concept is "direct signaling" of EVs where factors located at the surface of EVs can change the physiology of target cells (40,41). To investigate this possibility, we blocked EV endocytosis in MSCs using dynasore and subsequently incubated MSCs with PKH67-labeled 143B EVs for 24h. Although dynasore treatment decreased 143B EV internalization by more than 60%, EV-mediated induction of IL-6 MSCs was not affected (Figure 4d), suggesting that this is not fully dependent on EV internalization by MSCs.

It has been recently shown that several growth factors, such as TNFα, FGF and TGFβ, can be detected in association with EVs (42–44). TGFβ is a pleiotropic cytokine highly expressed by high-grade osteosarcoma (45) and presumably functions as an autocrine growth factor for osteosarcoma (46). Apart from the well-established actions of soluble TGFβ, a vesicle-associated form of TGFβ has been implicated in the stimulation of cytokine production and cancer progression (44). We quantified TGFβ1 in osteosarcoma EVs by ELISA and found high protein levels in osteosarcoma EVs compared to non-malignant fibroblast control vesicles (143B EVs: 593,9±29,5 pg/ml; hF EVs: 146,1±15,5 pg/ml) (Figure 4e). Importantly, blocking TGFβ signaling in MSCs by means of a TGFβ type I receptor (ALK) inhibitor strongly decreased EV-mediated IL-6 induction in MSCs (Figure 4f, Supplementary figure 3a,b). Addition of recombinant soluble TGFβ (sTGFβ) to MSC cultures did not reproduce IL-6 induction in the MSCs (Figure 4f, Supplementary figure 3a,b). These observations implicate the EV-associated form of TGFβ in the pro-metastatic inflammatory loop established by osteosarcoma EVs.

Blocking IL-6 signaling abrogates the pro-tumorigenic effects of TEMSCs in vivo

We then asked whether an anti-IL-6R antibody (tocilizumab) could reverse the effects of TEMSCs on tumor progression. Mice bearing bioluminescent osteosarcoma xenografts were injected with TEMSCs 2 days after tumor cell orthotopic inoculation. Tocilizumab (100 μg/mouse) was administered i.p. one day after tumor cell inoculation and every other day until the end of the experiment. Mice receiving non-educated MSCs and no MSCs (not shown) were used as control groups. We found that tocilizumab reduced tumor growth as early as day 10 after inoculation with osteosarcoma cells (Figure 5a,b). Of note, mice receiving tocilizumab treatment displayed BLI signals that overlapped with control groups receiving control MSCs.
It is well-established that the pro-oncogenic effects of IL-6 are mediated by STAT3, which links inflammation to cancer (47). We observed that TEMSCs induce an increase in nuclear STAT3 phosphorylation in tumor tissues, which was prevented by the concurrent administration of tocilizumab (Figure 5c,d, Supplementary figure 3c). Most importantly, the administration of tocilizumab reverted the pro-metastatic effects of TEMSCs in vivo (Figure 5e,f). Collectively, these data show that tumor EVs activate a pro-metastatic IL-6/STAT3 signaling axis in osteosarcoma by engaging MSCs (Figure 5g). However, we cannot rule out a possible contribution of mouse IL-6 to cancer progression in our model, as the anti-IL6 receptor antibody would also prevent the potential cross-reaction between mouse IL-6 and human IL-6R.

OS patients present active IL-6/STAT3 and TGFβ signaling and elevated levels of circulating EV-associated TGFβ

To confirm the role of IL-6/STAT3 signaling in primary osteosarcoma tissues, we first analyzed the IL-6 mRNA expression in 84 pre-treatment high-grade osteosarcoma diagnostic biopsies using a publicly available dataset (48) in the R2 Genomics Analysis and Visualization Platform (http://r2.amc.nl). In accordance with our in vitro data, IL-6 mRNA levels in osteosarcoma biopsies were low compared to osteoblasts, MSCs and bone tissue (Figure 6a). However, the immunohistochemical analysis of osteosarcoma tissue microarrays (TMA) revealed pSTAT3 nuclear staining in 65% of biopsies (n= 103, cut-off: 5% positive cells/tumor tissue) (Figure 6b), suggesting that STAT3 activation in tumor tissues is most likely determined by an exogenous source of IL-6.

To confirm these data we performed RNA-seq analysis of osteosarcoma tissues and surrounding bone of 18 osteosarcoma patients (Supplementary table 1). Again, IL-6 expression was relatively low in tumors and does not significantly differ from that of normal bone (mean rpm: 11.71 ± 3.4 vs 9.6 ± 2.9) (Supplementary figure 4a). Curiously, TGFβ mRNA was also not differentially expressed between normal and tumor tissues (Supplementary figure 4b), while multiple TGFβ-induced genes were strongly upregulated (Figure 6c,d, Supplementary figure 4c,d, Supplementary table 2). Among these, COL11A1 and TGFβI were the top two up-regulated genes in the analysis (log2 FC 1.51, p=1.06E-14 and log2 FC 1.40, p=1.35E-11 respectively). Gene set enrichment analysis (GSEA) of the top up-regulated genes in osteosarcoma tumors (log2 FC>1, p<0.0001) showed an overlap with 4 extracellular matrix genes early induced by TGFβ in fibroblasts (49). These include three collagen genes identified as definite TGFβ/SMAD3 targets (COL3A1, COL6A1, COL6A3), and MMP14 (Figure 6d). In support of the role of TGFβ in osteosarcoma, elevated TGFβ mRNA in high-grade osteosarcoma biopsies is associated with a decrease in metastasis free survival of osteosarcoma patients (Supplementary figure 4e).

Finally, we examined whether osteosarcoma patients have increased levels of membrane-bound TGFβ in circulation. To this end we purified EVs from patient serum (Supplementary table 3) using size-exclusion chromatography and quantified TGFβ levels by ELISA. Our analysis revealed that serum levels of EV-associated TGFβ are significantly higher in osteosarcoma patients compared to healthy control individuals (277.5 ± 35.3 vs 119.3 ± 39.1 pg/ml) (Figure 6e). To evaluate how well TGFβ levels discriminate between osteosarcoma patients and healthy individuals we used a ROC (Receiver Operating Characteristic) curve and obtained an AUC (area under the curve) score of 0.88 (Figure 6f). These data suggest that these TGFβ-carrying vesicles, arguably of tumor origin, might act on stromal and tumor cells to sustain cancer progression.

Discussion

Tumor secreted EVs promote metastasis formation in various mouse models. Using a bioluminescent orthotopic xenograft mouse model of osteosarcoma, we show that tumor cells instruct MSCs to activate an oncogenic IL6-STAT3 signaling axis, which is consistent with MSC receptiveness to local stimuli (9–12,16). We demonstrate that the osteosarcoma-secreted EVs carry functional TGFβ molecules that interact with MSCs and alter their behavior to promote tumor growth and metastasis formation. Our observations suggest that blocking IL-6 and TGFβ signaling might represent a valid therapeutic strategy for osteosarcoma.

Tumor-derived EVs can contribute to malignant progression by aiding in the formation of the pre-metastatic niche (20,50,51). This process may involve the education of bone marrow-derived and/or local specialized cells that shape a favorable environment at the metastatic site for malignant cells to seed and grow (20,50,51). Moreover, others have shown that stromal cell EVs also participate in tumorigenesis by providing a favorable environment (52). We propose a third pro-tumorigenic EV-mediated mechanism by which tumor cell-secreted EVs act on defined subset of stromal cells directly at the primary tumor site establishing a local pro-inflammatory loop. We show that short-time ex vivo conditioning of MSCs by tumor EVs is sufficient to increase metastasis formation in vivo. The MSC-contribution to osteosarcoma metastasis formation is largely dependent on increased IL-6 expression, leading to the activation of the STAT3 oncogene in the primary bone tumor.

In various cancer types, chronic or even short activation of the IL-6/STAT3 axis is a key event in cancer development and progression (53). IL-6/STAT3 signaling supports cancer cell proliferation, metastasis formation, tumor immunosuppression and cancer stem cell self-renewal (47). In addition, overexpression of IL-6 and its receptor (IL-6R) is observed frequently in multiple cancer types (54). Osteosarcoma patients seem to have high IL-6 serum levels compared to control individuals (55,56), and sustain activated intra-tumor STAT3 signaling as we demonstrate in this study (Figure 6b). Surprisingly, osteosarcoma tumor cells in vivo, primary osteosarcoma cells cultured in vitro as well as most osteosarcoma cell-lines that we studied express low to virtually undetectable levels of IL-6 (Figure 3b, Figure 6a, and Supplementary figure 4a). These observations, combined with the activated STAT3 signaling observed in osteosarcoma tumors, suggests that an exogenous source of IL-6 must be involved, strengthening the notion that tumors progress with the support of the microenvironment (8).

The complexity and heterogeneity of EVs complicates the identification of biomolecules that modify the physiology of recipient cells. We and others previously showed that both tumor EV-protected small RNAs and virus-derived small RNAs can induce inflammatory responses in target cells by triggering intracellular RNA sensors (32,38,39). Although we found that MSCs express functional endosomal TLRs, they are unresponsive to isolated tumor EV-RNA suggesting that IL-6 induction in response to osteosarcoma EVs is mediated by alternative mechanisms. Multiple EV-associated proteins including proto-oncogenes and heat-shock proteins have been implicated in the intercellular communication networks that support cancer progression (20,23). Depending on their localization EV-associated proteins might not require internalization by target cells to signal. However, until now, conclusions on EV function and tropism have been mostly drawn based on vesicle uptake by recipient cells (20,21,33,50–52). We demonstrate that osteosarcoma EVs alter MSC physiology independently of internalization, by carrying membrane-associated TGFβ to the surface of MSCs, where TGFβ interacts with the ALKV receptor (Figure 4d-f).

TGFβ is a key molecule in many metastasis models (57), and has a central role in the communication between cancer and stromal cells leading to disease progression (58). In osteosarcoma TGFβ has been previously implicated as an autocrine growth factor. Indeed, TGFβ mRNA expression in osteosarcoma tissues associates with high-grade tumors (45) and negatively correlates with metastasis-free survival (R2: Genomics Analysis and Visualization Platform, Kuijjer dataset). We show that in osteosarcoma patients metastasis-associated TGFβ-induced genes are overexpressed in the tumor tissue compared to the surrounding normal bone (Supplementary table 2). Intriguingly we could not detect differential expression of TGFβ, at least at the mRNA level (Supplementary Figure 4b). This suggests that TGFβ, secreted in a latent form, is activated within the tumor mass more so than in the surrounding normal bone tissue. An alternative explanation is that the levels of EV-bound TGFβ, rather than the total amount of TGFB protein, ultimately determines downstream target gene expression. In fact, we demonstrate that malignant osteosarcoma EVs carry high levels of membrane-bound TGFβ compared to EVs secreted by non-transformed cells (Figure 4e), which corresponds with their ability to educate MSCs to produce IL-6 (Figure 3c). Importantly, soluble TGFβ did not reproduce the effects induced by the EV-associated form on the MSCs (Figure 4f, Supplementary figure 3a,b), a finding supported by recent independent studies (44,59). Thus, a growth factor in association with EVs has distinct signaling properties than its soluble form (40,41). We propose that the conformation acquired by TGFβ on the EV surface, the combination with other EV-associated factors, or the presence of co-stimulatory signals on tumor EVs (59), might enhance or alter TGFβ signaling properties.

To demonstrate the clinical significance of vesicle-associated TGFβ in osteosarcoma, we quantified the levels of EV-bound TGFβ in human serum. We found that osteosarcoma patients have much higher levels of EV-associated TGFβ compared to healthy control individuals. Arguably, multiple cell types, including immune cells, might be exposed to the high levels of local or systemic EV-bound TGFβ in osteosarcoma patients. While the use of a xenograft mouse model allows to study the interactions between cell types of human origin in vivo, it limits the possibility to investigate the contribution of immune components such as tumor-infiltrating T cells to osteosarcoma progression. Further studies using syngeneic mouse models need to be performed to obtain a more complete picture of tumor-stromal cell interactions in osteosarcoma and to evaluate the potential role of EV-associated TGFβ and IL-6 in tumor immune escape.

Currently, adolescent osteosarcoma patients receive one of the most aggressive treatment regimens, while prognosis in the presence of metastases remains discouraging (2). This is the first study addressing the role of EV-mediated tumor-stroma communication in osteosarcoma. We describe the establishment of a pro-metastatic inflammatory loop initiated by osteosarcoma EVs that can be disrupted to inhibit osteosarcoma progression. This is relevant because IL-6 and TGFβ inhibitors are novel attractive targets for anti-cancer therapy (60,61). In particular, the anti-IL-6R antibody used in this study (tocilizumab), already approved for the treatment of rheumatic diseases, has been evaluated with encouraging results in a phase I trial for recurrent ovarian cancer (NCT01637532), and will be tested for the treatment of pancreatic cancer (NCT02767557) and Chronic Lymphocytic Leukemia (NCT02336048). Osteosarcoma is a rare tumor of childhood and adolescence, which complicates large clinical studies stressing the need for pre-clinical models. While it is unlikely that IL-6 blocking antibodies, used as single therapeutic agents, may result in patient response, combination with current chemotherapy treatment may improve osteosarcoma survival and allow to lower the dosage of

chemotherapeutic drugs, reducing toxicity. Moreover, our findings suggest that combination of IL-6 blocking agents with TGFβ inhibitors might halt osteosarcoma progression while reducing resistance.

Acknowledgements

The authors thank H. W. M. Niessen (VUmc, Amsterdam) for the provision of human MSCs; J.M. Middeldorp (VUmc, Amsterdam) for human fibroblasts; VW van Beusechem (VUmc, Amsterdam) for providing primary osteosarcoma cells; A. Avan and E. Giovannetti (VUmc, Amsterdam) for their support in the in vivo experimentation; G. Bonuccelli (Istituto Ortopedico Rizzoli, Bologna) for her assistance in tissue staining; J. Letterio (UH Cleveland Medical Center, Cleveland) for constructive discussion.

This work was supported by grants from the Italian Association for Cancer Research (AIRC, grant No 16159), the Veronesi Foundation, the L'Oréal-UNESCO "For Women in Science" and Marie Curie Actions (grant No 660200) to S.R.B., the Dutch Cancer Society (KWF, grant No VU2012-5510) to D.M.P., and the Italian Association for Cancer Research (AIRC, grant No 15608) to N.B..

References

1. Messerschmitt PJ, Garcia RM, Abdul-Karim FW, Greenfield EM, Getty PJ. Osteosarcoma. J Am Acad Orthop Surg. 2009;17:515–27.
2. Kansara M, Teng MW, Smyth MJ, Thomas DM. Translational biology of osteosarcoma. Nat Rev Cancer. Nature Publishing Group, a division of Macmillan Publishers Limited. All Rights Reserved.; 2014;14:722–35.
3. Stephens PJ, Greenman CD, Fu B, Yang F, Bignell GR, Mudie LJ, et al. Massive genomic rearrangement acquired in a single catastrophic event during cancer development. Cell. 2011;144:27–40.
4. Rubio R, Abarrategi A, Garcia-Castro J, Martinez-Cruzado L, Suarez C, Tornin J, et al. Bone environment is essential for osteosarcoma development from transformed mesenchymal stem cells. Stem Cells. 2014;32:1136–48.
5. Alfranca A, Martinez-Cruzado L, Tornin J, Abarrategi A, Amaral T, de Alava E, et al. Bone microenvironment signals in osteosarcoma development. Cell Mol Life Sci. 2015;72:3097–113.
6. Ottaviani G, Jaffe N. The epidemiology of osteosarcoma. Cancer Treat Res. 2009;152:3–13.
7. Longhi A, Pasini A, Cicognani A, Baronio F, Pellacani A, Baldini N, et al. Height as a risk factor for osteosarcoma. J Pediatr Hematol Oncol. 2005;27:314–8.
8. Hanahan D, Weinberg RA. Hallmarks of cancer: The next generation. Cell. 2011. page 646–74.
9. Karnoub AE, Dash AB, Vo AP, Sullivan A, Brooks MW, Bell GW, et al. Mesenchymal stem cells within tumour stroma promote breast cancer metastasis. Nature. 2007;449:557–63.
10. Behnan J, Isakson P, Joel M, Cilio C, Langmoen IA, Vik-Mo EO, et al. Recruited brain tumor-derived mesenchymal stem cells contribute to brain tumor progression. Stem Cells. 2014;32:1110–23.
11. Shinagawa K, Kitadai Y, Tanaka M, Sumida T, Onoyama M, Ohnishi M, et al. Stroma-directed imatinib therapy impairs the tumor-promoting effect of bone marrow-derived mesenchymal stem cells in an orthotopic transplantation model of colon cancer. Int J Cancer. 2012;132:813–23.
12. Xu W, Bian Z, Fan Q, Li G, Tang T. Human mesenchymal stem cells (hMSCs) target osteosarcoma and promote its growth and pulmonary metastasis. Cancer Lett. 2009;281:32–41.
13. Barcellos-de-Souza P, Gori V, Bambi F, Chiarugi P. Tumor microenvironment: bone marrow-mesenchymal stem cells as key players. Biochim Biophys Acta. 2013;1836:321–35.
14. Luo J, Ok Lee S, Liang L, Huang C-K, Li L, Wen S, et al. Infiltrating bone marrow mesenchymal stem cells increase prostate cancer stem cell population and metastatic ability via secreting cytokines to suppress androgen receptor signaling. Oncogene. 2013;33:2768–78.
15. Huang W-H, Chang M-C, Tsai K-S, Hung M-C, Chen H-L, Hung S-C. Mesenchymal stem cells promote growth and angiogenesis of tumors in mice. Oncogene. 2013;32:4343–54.
16. Jung Y, Kim JK, Shiozawa Y, Wang J, Mishra A, Joseph J, et al. Recruitment of mesenchymal stem cells into prostate tumours promotes metastasis. Nat Commun. Nature Publishing Group, a division of Macmillan Publishers Limited. All Rights Reserved.; 2013;4:1795.
17. Trajkovic K, Hsu C, Chiantia S, Rajendran L, Wenzel D, Wieland F, et al. Ceramide triggers budding of exosome vesicles into multivesicular endosomes. Science. 2008;319:1244–7.
18. Skog J, Würdinger T, van Rijn S, Meijer DH, Gainche L, Sena-Esteves M, et al. Glioblastoma microvesicles transport RNA and proteins that promote tumour growth and provide diagnostic

biomarkers. Nat Cell Biol. 2008;10:1470–6.

19. Kowal J, Arras G, Colombo M, Jouve M, Morath JP, Primdal-Bengtson B, et al. Proteomic comparison defines novel markers to characterize heterogeneous populations of extracellular vesicle subtypes. Proc Natl Acad Sci U S A. 2016;113:E968-77.

20. Peinado H, Alečković M, Lavotshkin S, Matei I, Costa-Silva B, Moreno-Bueno G, et al. Melanoma exosomes educate bone marrow progenitor cells toward a pro-metastatic phenotype through MET. Nat Med. 2012;18:883–91.

21. Zomer A, Maynard C, Verweij FJ, Kamermans A, Schäfer R, Beerling E, et al. In Vivo Imaging Reveals Extracellular Vesicle-Mediated Phenocopying of Metastatic Behavior. Cell. 2015;161:1046–57.

22. Zhuang G, Wu X, Jiang Z, Kasman I, Yao J, Guan Y, et al. Tumour-secreted miR-9 promotes endothelial cell migration and angiogenesis by activating the JAK-STAT pathway. EMBO J. 2012. page 3513–23.

23. Chalmin F, Ladoire S, Mignot G, Vincent J, Bruchard M, Remy-Martin J-P, et al. Membrane-associated Hsp72 from tumor-derived exosomes mediates STAT3-dependent immunosuppressive function of mouse and human myeloid-derived suppressor cells. J Clin Invest. 2010;120:457–71.

24. Melo SA, Luecke LB, Kahlert C, Fernandez AF, Gammon ST, Kaye J, et al. Glypican-1 identifies cancer exosomes and detects early pancreatic cancer. Nature. 2015;523:177–82.

25. Shao H, Chung J, Lee K, Balaj L, Min C, Carter BS, et al. Chip-based analysis of exosomal mRNA mediating drug resistance in glioblastoma. Nat Commun. 2015;6:6999.

26. Mohseny AB, Szuhai K, Romeo S, Buddingh EP, Briaire-de Bruijn I, de Jong D, et al. Osteosarcoma originates from mesenchymal stem cells in consequence of aneuploidization and genomic loss of Cdkn2. J Pathol. 2009;219:294–305.

27. Baranski Z, Booij TH, Cleton-Jansen A-M, Price LS, van de Water B, Bovée JVMG, et al. Aven-mediated checkpoint kinase control regulates proliferation and resistance to chemotherapy in conventional osteosarcoma. J Pathol. 2015;236:348–59.

28. Baglio SR, Rooijers K, Koppers-Lalic D, Verweij FJ, Pérez Lanzón M, Zini N, et al. Human bone marrow- and adipose-mesenchymal stem cells secrete exosomes enriched in distinctive miRNA and tRNA species. Stem Cell Res Ther. 2015;6:127.

29. Grisendi G, Bussolari R, Cafarelli L, Petak I, Rasini V, Veronesi E, et al. Adipose-derived mesenchymal stem cells as stable source of tumor necrosis factor-related apoptosis-inducing ligand delivery for cancer therapy. Cancer Res. 2010;70:3718–29.

30. van Eijndhoven MAJ, Zijlstra JM, Groenewegen NJ, Drees EEE, van Niele S, Baglio SR, et al. Plasma vesicle miRNAs for therapy response monitoring in Hodgkin lymphoma patients. JCI Insight. 2016;1:e89631.

31. Love MI, Huber W, Anders S. Moderated estimation of fold change and dispersion for RNA-seq data with DESeq2. Genome Biol. 2014;15:550.

32. Baglio SR, van Eijndhoven MAJ, Koppers-Lalic D, Berenguer J, Lougheed SM, Gibbs S, et al. Sensing of latent EBV infection through exosomal transfer of 5'pppRNA. Proc Natl Acad Sci U S A. 2016;

33. Pucci F, Garris C, Lai CP, Newton A, Pfirschke C, Engblom C, et al. SCS macrophages suppress melanoma by restricting tumor-derived vesicle-B cell interactions. Science (80-). 2016;352:242–6.

34. Dvorak HF. Tumors: wounds that do not heal. Similarities between tumor stroma generation and wound healing. N Engl J Med. 1986;315:1650–9.

35. Reagan MR, Kaplan DL. Concise Review: Mesenchymal Stem Cell Tumor-Homing: Detection Methods in Disease Model Systems. Stem Cells. Wiley Subscription Services, Inc., A Wiley Company; 2011;29:920–7.

36. Bernardo ME, Fibbe WE. Mesenchymal stromal cells: sensors and switchers of inflammation. Cell Stem Cell. 2013;13:392–402.

37. Pricola KL, Kuhn NZ, Haleem-Smith H, Song Y, Tuan RS. Interleukin-6 maintains bone marrow-derived mesenchymal stem cell stemness by an ERK1/2-dependent mechanism. J Cell Biochem. 2009;108:577–88.

38. Fabbri M, Paone A, Calore F, Galli R, Gaudio E, Santhanam R, et al. MicroRNAs bind to Toll-like receptors to induce prometastatic inflammatory response. Proc Natl Acad Sci U S A. 2012;109:E2110-6.

39. Boelens MC, Wu TJ, Nabet BY, Xu B, Qiu Y, Yoon T, et al. Exosome transfer from stromal to breast cancer cells regulates therapy resistance pathways. Cell. 2014;159:499–513.

40. Cossetti C, Iraci N, Mercer TR, Leonardi T, Alpi E, Drago D, et al. Extracellular vesicles from neural stem cells transfer IFN-γ via Ifngr1 to activate Stat1 signaling in target cells. Mol Cell. 2014;56:193–204.

41. Szczepanski MJ, Szajnik M, Welsh A, Whiteside TL, Boyiadzis M. Blast-derived microvesicles in sera from patients with acute myeloid leukemia suppress natural killer cell function via membrane-associated transforming growth factor-β1. Haematologica. 2011;96.

42. Zhang H-G, Liu C, Su K, Su K, Yu S, Zhang L, et al. A membrane form of TNF-alpha presented by exosomes delays T cell activation-induced cell death. J Immunol. 2006;176:7385–93.

43. Seelenmeyer C, Stegmayer C, Nickel W. Unconventional secretion of fibroblast growth factor 2 and galectin-1 does not require shedding of plasma membrane-derived vesicles. FEBS Lett. 2008;582:1362–8.

44. Webber J, Steadman R, Mason MD, Tabi Z, Clayton A. Cancer exosomes trigger fibroblast to myofibroblast differentiation. Cancer Res. 2010;70:9621–30.

45. Expression of transforming growth factor beta isoforms in osteosarcoma variants: association of TGF beta 1 with high-grade osteosarcomas. - PubMed - NCBI [Internet]. [cited 2015 Oct 5]. Available from: http://www.ncbi.nlm.nih.gov/pubmed/9771482

46. Kloen P, Jennings CL, Gebhardt MC, Springfield DS, Mankin HJ. Expression of transforming growth factor-beta (TGF-beta) receptors, TGF-beta 1 and TGF-beta 2 production and autocrine growth control in osteosarcoma cells. Int J cancer. 1994;58:440–5.

47. Yu H, Lee H, Herrmann A, Buettner R, Jove R. Revisiting STAT3 signalling in cancer: new and unexpected biological functions. Nat Rev Cancer. 2014;14:736–46.

48. Kuijjer ML, Hogendoorn PCW, Cleton-Jansen A-M. Genome-wide analyses on high-grade osteosarcoma: making sense of a genomically most unstable tumor. Int J cancer. 2013;133:2512–21.

49. Verrecchia F, Chu ML, Mauviel A. Identification of novel TGF-beta /Smad gene targets in dermal fibroblasts using a combined cDNA microarray/promoter transactivation approach. J Biol Chem. 2001;276:17058–62.

50. Costa-Silva B, Aiello NM, Ocean AJ, Singh S, Zhang H, Thakur BK, et al. Pancreatic cancer exosomes initiate pre-metastatic niche formation in the liver. Nat Cell Biol. Nature Research; 2015;17:816–26.

51. Hoshino A, Costa-Silva B, Shen T-L, Rodrigues G, Hashimoto A, Tesic Mark M, et al. Tumour exosome integrins determine organotropic metastasis. Nature. 2015;527:329–35.

52. Zhang L, Zhang S, Yao J, Lowery FJ, Zhang Q, Huang W-C, et al. Microenvironment-induced PTEN loss by exosomal microRNA primes brain metastasis outgrowth. Nature. 2015;527:100–4.

53. Iliopoulos D, Hirsch HA, Struhl K. An epigenetic switch involving NF-kappaB, Lin28, Let-7 MicroRNA, and IL6 links inflammation to cell transformation. Cell. 2009;139:693–706.

54. Guo Y, Xu F, Lu T, Duan Z, Zhang Z. Interleukin-6 signaling pathway in targeted therapy for cancer. Cancer Treat Rev. 2012;38:904–10.

55. Xiao H, Chen L, Luo G, Son H, Prectoni JH, Zheng W. Effect of the cytokine levels in serum on osteosarcoma. Tumour Biol. 2014;35:1023–8.

56. Rutkowski P, Kamińska J, Kowalska M, Ruka W, Steffen J. Cytokine and cytokine receptor serum levels in adult bone sarcoma patients: correlations with local tumor extent and prognosis. J Surg Oncol. 2003;84:151–9.

57. Padua D, Massagué J. Roles of TGFbeta in metastasis. Cell Res. 2009;19:89–102.

58. Calon A, Lonardo E, Berenguer-Llergo A, Espinet E, Hernando-Momblona X, Iglesias M, et al. Stromal gene expression defines poor-prognosis subtypes in colorectal cancer. Nat Genet. Nature Research; 2015;47:320–9.

59. Webber JP, Spary LK, Sanders AJ, Chowdhury R, Jiang WG, Steadman R, et al. Differentiation of tumour-promoting stromal myofibroblasts by cancer exosomes. Oncogene. 2015;34:290–302.

60. Rossi J-F, Lu Z-Y, Jourdan M, Klein B. Interleukin-6 as a therapeutic target. Clin Cancer Res. 2015;21:1248–57.

61. Neuzillet C, Tijeras-Raballand A, Cohen R, Cros J, Faivre S, Raymond E, et al. Targeting the TGFβ pathway for cancer therapy. Pharmacol Ther. 2015;147:22–31.

Figure legends

Figure 1. Osteosarcoma cell lines release exosome-like vesicles that can be internalized by MSCs. (A) CD63 (green) and lysosome (red) fluorescence staining (top), and ultrastructure of MVB-like endosomes (bottom) in MG63, HOS and 143B osteosarcoma cell lines (scale bar: 100 nm). (B) Transmission electron microscopy micrographs of EVs isolated from osteosarcoma cell lines (scale bar: 100 nm). (C) Western blot for CD63 and CD81 in osteosarcoma cells and corresponding EVs. (D) Internalization of PKH67-labeled EVs by MSCs assessed by fluorescence microscopy (top) and FACS analysis (bottom).

Figure 2. Tumor EV-educated MSCs promote tumor growth and metastasis formation in a bioluminescent orthotopic xenograft model of osteosarcoma. (A) Schematic representation of the experimental design: luciferase-positive human metastatic osteosarcoma (143B) cells were inoculated in the tibia of immunocompromised mice; human GFP-positive MSCs were educated with osteosarcoma (143B)-released EVs for 48 hours, and educated (TEMSC) or non-educated MSCs were systemically injected in the osteosarcoma-bearing mice. Mice receiving no MSCs were used as controls. (B) Tumor growth measured by bioluminescence imaging (BLI) over the experimental time-frame in mice receiving TEMSCs, control MSCs or no MSCs (two independent experiments, n=6/group/experiment) ($p < 0.05$ TEMSC vs MSC, LSD test). (C) Representative BLI images of mice receiving TEMSCs, control MSCs or no MSCs. (D) Immunofluorescence staining of GFP-positive MSCs in the bone marrow and tumor tissue of MSC-receiving mice. (E) Representative ex vivo BLI images of lung, liver and spleen of mice receiving TEMSCs, control MSCs or no MSCs. (F) Lung metastasis number assessed by ex vivo BLI in the different experimental groups (two independent experiments, n=6/group) ($p < 0.05$, LSD test). (G) HE and human vimentin staining of lung metastasis in osteosarcoma-bearing mice.

Figure 3. Osteosarcoma EVs induce IL-6 production and promote cell cycle progression in human MSCs. (A) Multiplexed bead-based protein detection of inflammatory cytokines in the culture supernatant of MSCs exposed to human fibroblast (hF) or 143B EVs. (B) IL-6 protein detection in the conditioned medium (CM) of osteosarcoma cell lines, primary osteosarcoma cells (Prim-OS) and control fibroblasts (hF), and indicated EVs by ELISA. (C) IL-6 protein detection in the conditioned medium (CM) of MSCs exposed to indicated EVs. The graph shows data from 3 independent experiments, data are expressed as fold induction relative to the untreated control (set at 1) ($p < 0.05$ 143B EVs vs untreated and 143B EVs vs hF EVs, t test). (D) sIL-6R protein detection in the conditioned medium of indicated cell types. (E) Cell cycle distribution of MSCs treated with 143B or control EVs upon mitotic arrest. For capturing cells in G2-M, prior to FACS analysis EV-treated or untreated MSCs were incubated overnight with nocodazole. (F) Relative distribution of MSCs in G1 and G2-M phases. For each condition, the difference between EV-treated and untreated cells was calculated and plotted ($p<0.05$ 143B EV vs untreated control, t test).

Figure 4. A membrane-associated form of TGFβ on the surface of osteosarcoma EVs induces IL-6 expression in MSCs. (A) Bioanalyzer small RNA profile showing enrichment of 20–70 nucleotide RNA species in indicated osteosarcoma EVs. (B) Relative expression level of endosomal TLRs in MSCs analyzed by qPCR. Transcript levels are normalized to GAPDH. (C) Relative expression levels of IL-6 in MSCs transfected with osteosarcoma (143B) EV-RNA or poly I:C (positive control) (left), or treated with matching amounts of intact 143B EVs (right). Transcript levels are normalized to GAPDH and expressed as fold increase relative to the untreated control. (D) Assessment of internalization of PKH67-labeled 143B EVs in the presence or absence of dynasore by FACS (left).

Relative expression levels of IL-6 in MSCs treated with 143B EVs in the presence or absence of dynasore (right). Transcript levels are normalized to GAPDH and expressed as fold increase relative to the experimental controls (untreated or dynasore-treated). Three independent experiment were performed ($p < 0.05$, LSD test). (E) TGFβ protein detection in control fibroblasts (hF) and osteosarcoma (MG63, HOS and 143B) EVs by ELISA. (F) Relative expression levels of IL-6 in MSCs treated with soluble TGFβ (sTGFβ) or 143B EVs in the presence or absence of a TGFβ type I receptor (ALK) inhibitor (SB431542) at 24h. Transcript levels are normalized to GAPDH and expressed as fold increase relative to the untreated controls. Three independent experiment were performed ($p<0.05$, LSD test).

Figure 5. Treatment with an anti-IL-6R antibody abrogates the pro-tumorigenic and pro-metastatic effects of TEMSCs. (A) BLI analysis of tumor growth over the experimental time-frame in mice receiving non-educated MSCs, TEMSCs, or TEMSCs and IL-6R Ab (tocilizumab) (n=6/group). The anti-IL-6R antibody was administered starting from day 1 (green arrow) every other day until the end of the experiment (TEMSC vs MSC and TEMSC vs TEMSC + IL-6R Ab $p < 0.05$, LSD test). (B) Representative BLI images (top) and tumor pictures (bottom) of mice receiving non-educated MSCs, TEMSCs, or TEMSCs and anti-IL-6R antibody. (C) Representative images of nuclear pSTAT3 (red) by immunofluorescence staining in indicated tumors; nuclei are stained with DAPI (grey). (D) Quantification of pSTAT3 nuclear staining in tumor slices. Images from 3 mice/group were analyzed. Results are expressed as relative percentage of pSTAT3-positive nuclei over the total amount of (DAPI-stained) nuclei ($p < 0.05$, LSD test). (E) Lung metastasis number assessed by ex vivo BLI in the different experimental groups (n=6/group) ($p \leq 0.05$, LSD test). (F) Representative ex vivo BLI images of lung, liver and spleen of mice receiving non-educated MSCs, TEMSCs, or TEMSCs and anti-IL-6R antibody. (G) Schematic representation of the proposed model. Osteosarcoma cells release EVs decorated with a membrane-bound form of TGFβ that increases IL-6 production in MSCs. MSC-derived IL-6 increases tumor growth and metastasis formation in mice bearing osteosarcoma tumors. The pro-tumorigenic effects of IL-6-producing MSCs can be blocked by IL-6 signaling blocking agents (tocilizumab).

Figure 6. Osteosarcoma patients have activated STAT3 and TGFβ signaling and elevated levels of circulating TGFβ associated with EVs. (A) IL-6 mRNA expression in pre-treatment high-grade osteosarcoma diagnostic biopsies and indicated cell lines and tissues (Kuijjer dataset, R2: Genomics Analysis and Visualization Platform (http://r2.amc.nl)). (B) Representative image of immunohistochemical staining of pSTAT3 in pre-chemotherapy osteosarcoma tissue microarrays (TMA). (C and D) Normalized read counts of indicated TGFβ-induced genes in osteosarcoma tumors compared to surrounding normal bone tissue as analyzed by RNA-seq (n=18 patients). Data are expressed as reads per million (rpm). (E and F) Quantification of TGFβ protein levels in serum EVs from osteosarcoma patient and control donors by ELISA (n=10/group, $p < 0.05$, t test) (E) and relative ROC curve (AUC: 0.88, p=0.004) (F). OS: osteosarcoma.

Figure 1

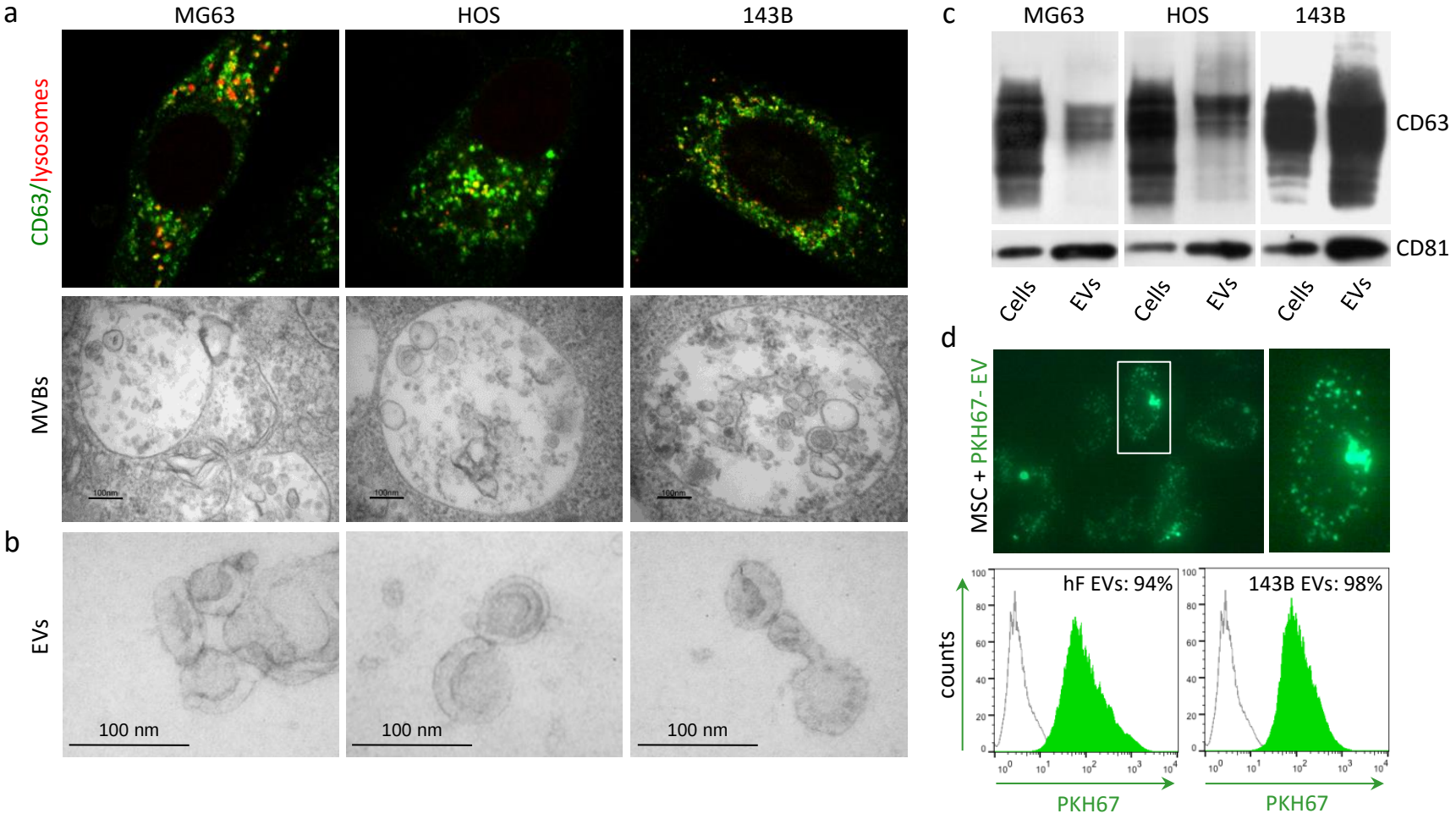
a
MG63
HOS
143B
CD63/lysosomes
MVBs
b
EVs
100 nm
100 nm
100 nm
c
MG63
HOS
143B
CD63
CD81
Cells
EVs
Cells
EVs
Cells
EVs
d
MSC + PKH67- EV
hF EVs: 94%
143B EVs: 98%
counts
PKH67
PKH67

Figure 2

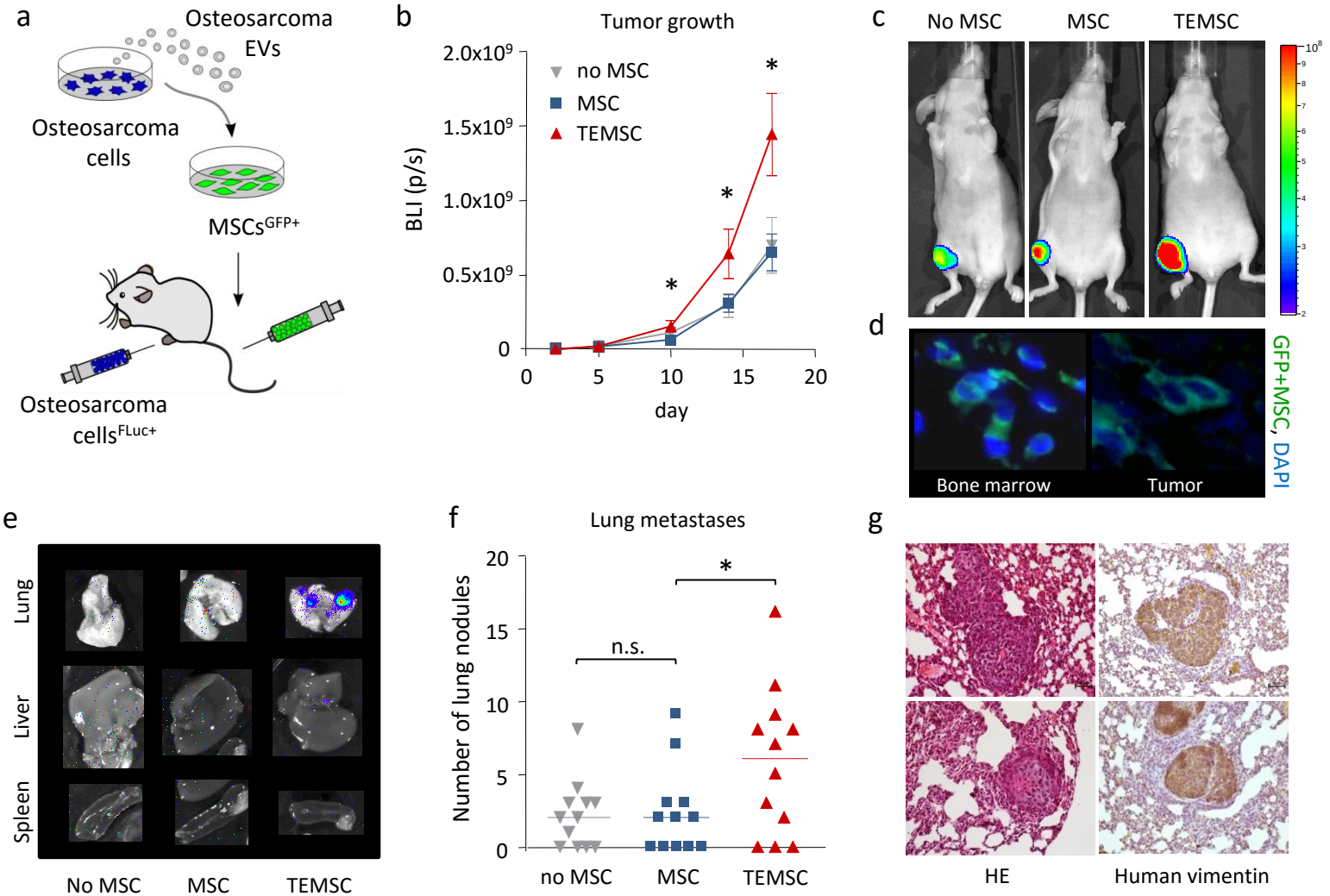
a
Osteosarcoma EVs
Osteosarcoma cells
MSCsGFP+
Osteosarcoma cellsFLuc+
b
Tumor growth
no MSC
MSC
TEMSC
BLI (p/s)
2.0x10^9
1.5x10^9
1.0x10^9
0.5x10^9
0
0
5
10
15
20
day
*
c
No MSC
MSC
TEMSC
d
Bone marrow
Tumor
GFP+MSC, DAPI
e
Lung
Liver
Spleen
No MSC
MSC
TEMSC
f
Lung metastases
Number of lung nodules
n.s.
*
no MSC
MSC
TEMSC
g
HE
Human vimentin

Figure 3

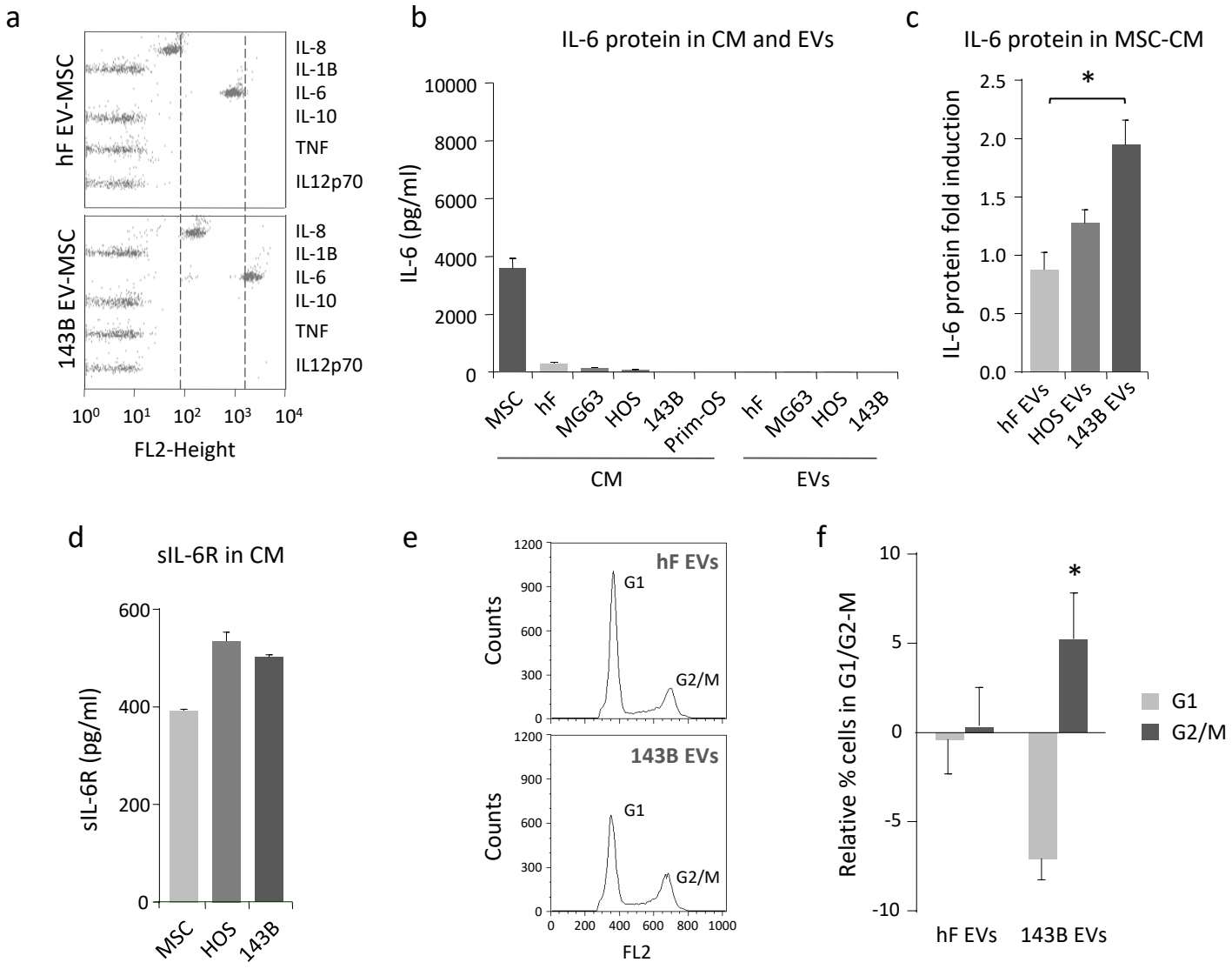
a
hF EV-MSC
143B EV-MSC
IL-8
IL-1B
IL-6
IL-10
TNF
IL12p70
10^0 10^1 10^2 10^3 10^4
FL2-Height
b
IL-6 protein in CM and EVs
IL-6 (pg/ml)
10000
8000
6000
4000
2000
0
MSC hF MG63 HOS 143B Prim-OS hF MG63 HOS 143B
CM
EVs
c
IL-6 protein in MSC-CM
IL-6 protein fold induction
2.5
2.0
1.5
1.0
0.5
0.0
*
hF EVs HOS EVs 143B EVs
d
sIL-6R in CM
sIL-6R (pg/ml)
600
400
200
0
MSC HOS 143B
e
hF EVs
143B EVs
Counts
G1
G2/M
1200
900
600
300
0
0 200 400 600 800 1000
FL2
f
Relative % cells in G1/G2-M
10
5
0
-5
-10
*
G1
G2/M
hF EVs 143B EVs

Figure 4

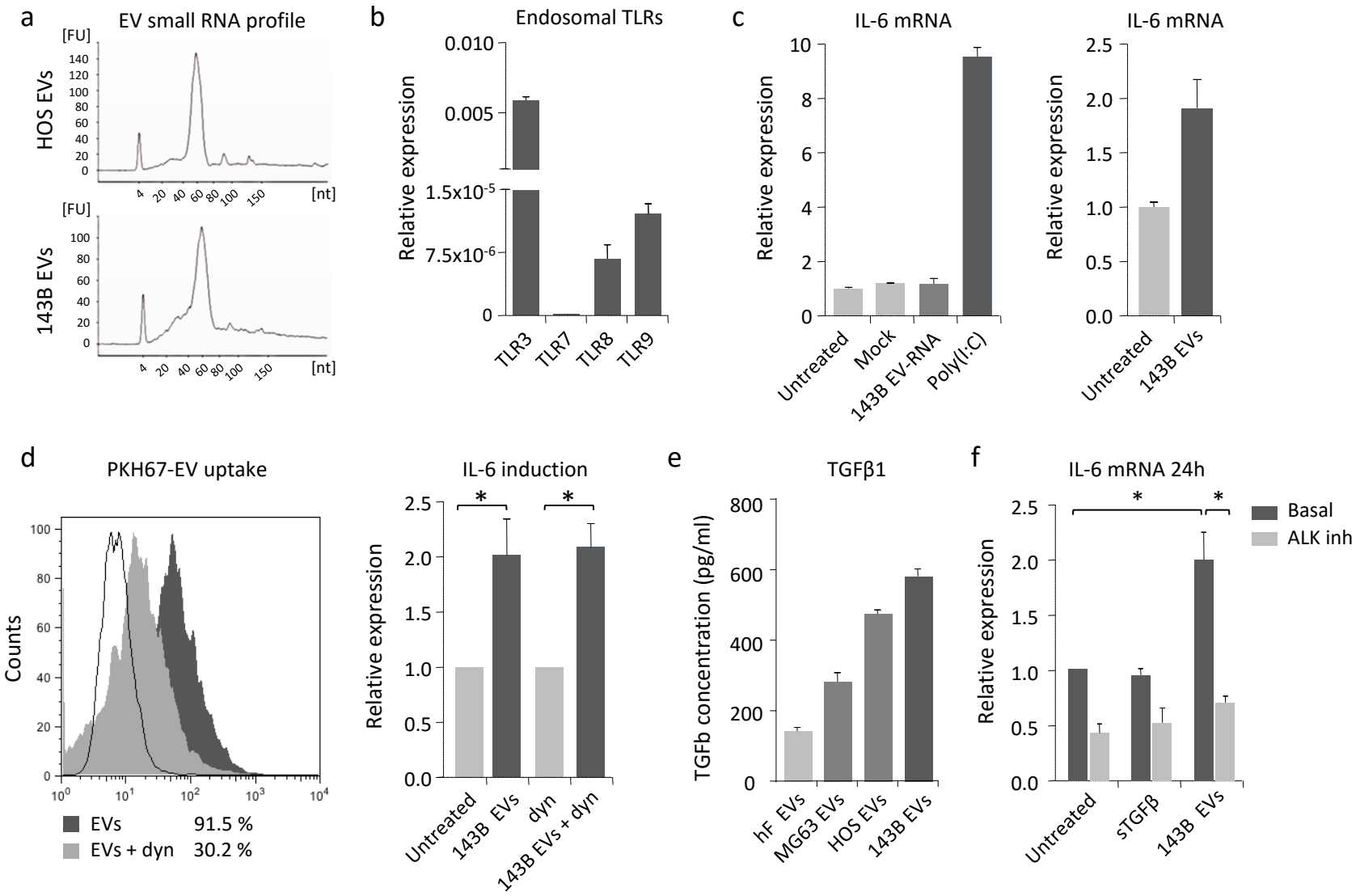
a
EV small RNA profile
HOS EVs
143B EVs
[FU]
[nt]
b
Endosomal TLRs
Relative expression
TLR3
TLR7
TLR8
TLR9
c
IL-6 mRNA
Relative expression
Untreated
Mock
143B EV-RNA
Poly(I:C)
IL-6 mRNA
Untreated
143B EVs
d
PKH67-EV uptake
Counts
EVs 91.5 %
EVs + dyn 30.2 %
IL-6 induction
Relative expression
Untreated
143B EVs
dyn
143B EVs + dyn
e
TGFβ1
TGFb concentration (pg/ml)
hF EVs
MG63 EVs
HOS EVs
143B EVs
f
IL-6 mRNA 24h
Relative expression
Basal
ALK inh
Untreated
sTGFβ
143B EVs

Figure 5

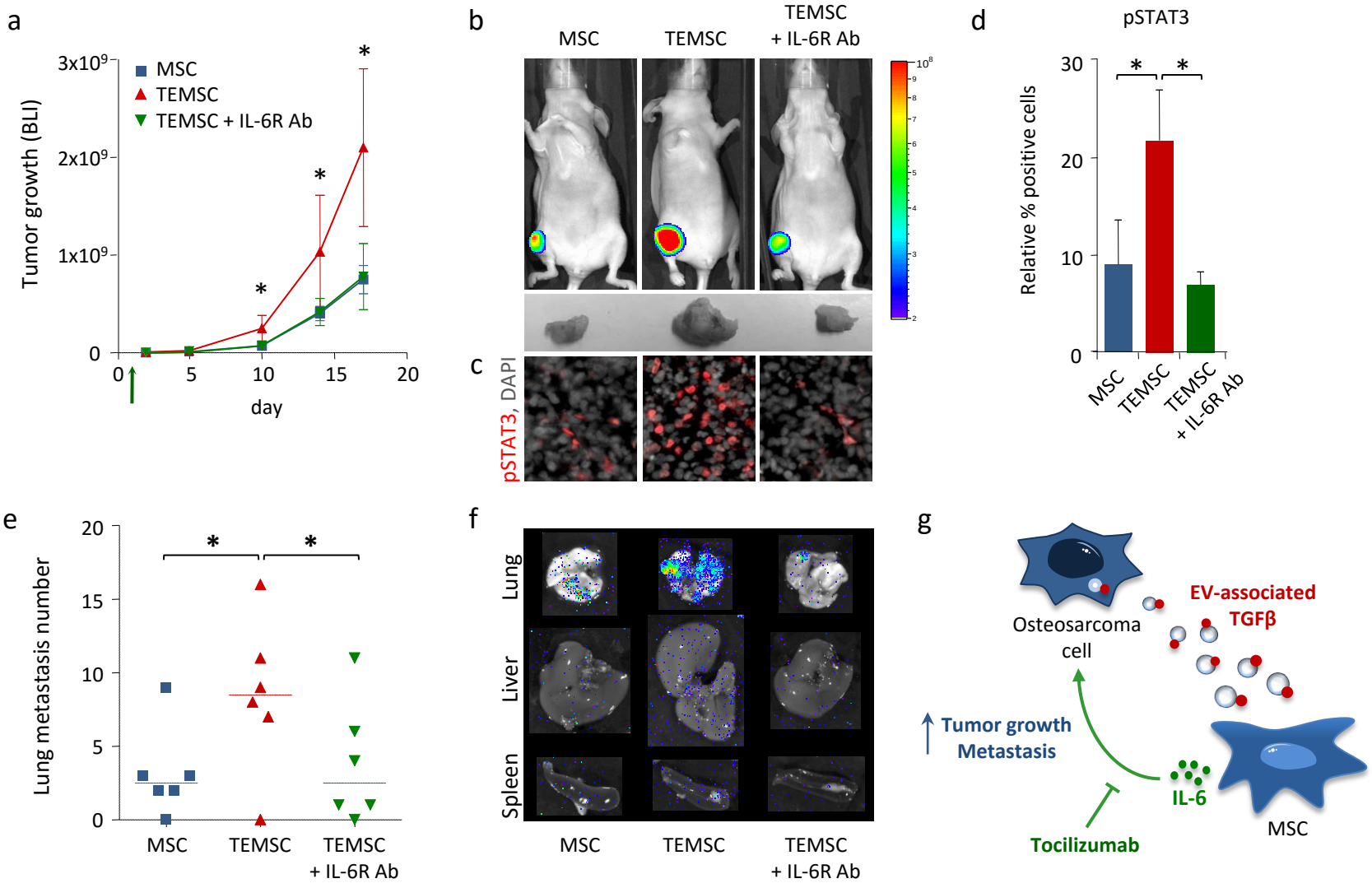
a
Tumor growth (BLI)
3x10⁹
2x10⁹
1x10⁹
0
MSC
TEMSC
TEMSC + IL-6R Ab
0
5
10
15
20
day
b
MSC
TEMSC
TEMSC + IL-6R Ab
c
pSTAT3, DAPI
d
pSTAT3
Relative % positive cells
30
20
10
0
MSC
TEMSC
TEMSC + IL-6R Ab
e
Lung metastasis number
20
15
10
5
0
MSC
TEMSC
TEMSC + IL-6R Ab
f
Lung
Liver
Spleen
MSC
TEMSC
TEMSC + IL-6R Ab
g
Osteosarcoma cell
EV-associated TGFβ
Tumor growth
Metastasis
IL-6
MSC
Tocilizumab

Figure 6

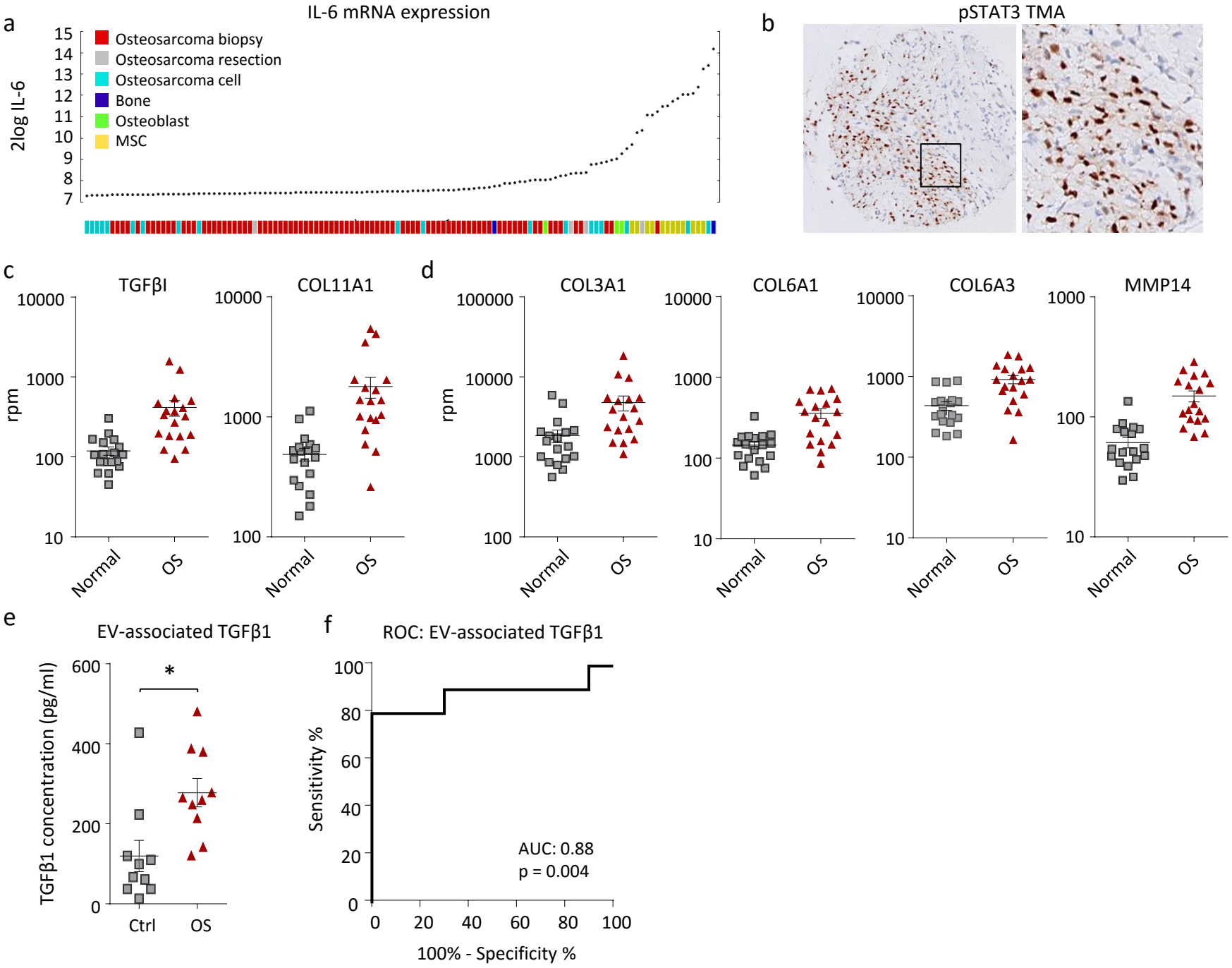
a
IL-6 mRNA expression
2log IL-6
Osteosarcoma biopsy
Osteosarcoma resection
Osteosarcoma cell
Bone
Osteoblast
MSC
b
pSTAT3 TMA
c
TGFβI
COL11A1
rpm
Normal
OS
d
COL3A1
COL6A1
COL6A3
MMP14
e
EV-associated TGFβ1
TGFβ1 concentration (pg/ml)
Ctrl
OS
f
ROC: EV-associated TGFβ1
Sensitivity %
100% - Specificity %
AUC: 0.88
p = 0.004